Search for K^- Mass Modification in the Nuclear Medium with Sub-threshold $^{12}C(e,e'K^{\pm})$ Processes

B. Clasie, C. Crawford, D. Dutta (spokesperson/contact person), H. Gao (spokesperson),

C. Seely, C. F. Williamson, H. Xiang, F. Xiong, W. Xu, L. Y. Zhu

Massachusetts Institute of Technology, Cambridge, MA

F. Dohrmann (spokesperson)

Argonne National Lab, Argonne, IL

W. Boeglin, P. Markowitz, J. Reinhold

Florida International University, Miami, FL

O. K. Baker, L. G. Tang

Hampton University, Newport News, VA

R. De Leo

INFN-Bari, Italy

G. M. Urciuoli

INFN-Roma1, Rome, Italy

M. Iodice

INFN -Roma3, Rome, Italy

E. Cisbani, S. Frullani, F. Garibaldi, R. Iommi

ISS-Physics Lab & INFN - Sanita, Italy

J. P Chen, E. Chudakov, J. Gomez, J.-O. Hansen, C. W. de Jager, J. LeRose,

N. Liyanage, R. Michaels, J. Mitchell, A. Saha, B. Wojtsekhowski

Thomas Jefferson National Accelerator Facility, Newport News, VA

W. Korsch

University of Kentucky, Lexington, KY

J. Calarco

University of New Hampshire, Durham, NH

Hall A Collaboration Proposal

Abstract

Electroproduction of K^+ and K^- from nuclei below the free space production thresholds on the nucleon is an exciting, new probe of the predicted medium modification of K^- mass inside nuclei. We propose measurements in electroproduction of K^+ and K^- from liquid Hydrogen and solid Carbon targets at energy transfers ranging from 0.8 to 1.8 GeV which correspond to $K^\pm$ momenta of 0.3-0.4 GeV. The proposed measurement will at the same time allow a study of the short-range correlations by probing the high momentum components of the nuclear wave function. A total beam-time of 774 hours is requested for this experiment.

I. INTRODUCTION

In 1986 Kaplan and Nelson [1] pointed out the possibility for a kaon condensed phase in dense nuclear matter, arising out of the large explicit chiral symmetry breaking (which gives rise to the strange quark mass.) Ever since this pioneering work on the possibility of kaon condensation in nuclear matter, a significant amount of theoretical and experimental efforts has been devoted to the study of kaon properties in dense matter. The properties of the K^+ and K^- in the nuclear medium are essential in determining the possible occurrence of such kaon condensation which would have dramatic consequences in stellar collapse and neutron star cooling [2]. Extensive studies based on such diverse approaches as chiral perturbation theory [3], mean field theory [4] and Nambu-Jona-Lasino model [5] have suggested that in nuclear matter the K^+ feels a weak repulsive potential, whereas the K^- feels a strong attractive potential. This indicates that the K^+ effective mass increases in dense matter and it will not condense, however, the effective mass of K^- meson decreases with increasing nuclear density, leading to K^- condensation at densities above 3 times saturation density ρ_0. More importantly, all models suggest that the effective mass of the K^- is substantially lowered [2] even at normal nuclear density, which allows for sensitive experiments designed

to look for medium modification of the K^- at normal nuclear density.

Apart from being interesting in its own right because of its direct bearing on explicit and spontaneous chiral symmetry breaking, medium effects of the K^- have many important consequences, such as in the dynamics of supernovae, and in the collapse and cooling of neutron stars and their transitions to black holes [6,7]. Medium effects, particularly K^- condensates, substantially reduce the maximum mass of neutron stars and thus provide a mechanism for the formation of low mass black holes [6]. Therefore the confirmation of these medium effects deserves special efforts.

Experimentally, in-medium properties of $K^\pm$ were first studied in kaon-nucleus scattering [8,9] and kaonic atoms [10]. These experiments found evidence for the attractive in-medium K^-N potential, but were restricted to very low densities accessible by kaonic atoms. Heavy-ion collision experiments, on the other hand, were able to access higher densities and a few experiments have seen hints of modification of the K^- properties in the nuclear medium [11]. Electroproduction of K^+ and K^- can be a new alternative probe which would allows us to investigate possible modification of the K^- properties in the nuclear medium. A novel experimental technique based on measuring the super-ratio of K^- to K^+ below and above their respective free space production thresholds is presented in this proposal. The motivation for the experiment is to investigate the possible medium modification of the K^- mass in sub-threshold electroproduction of $K^\pm$ from nuclei. As a bonus the sub-threshold K^+ production data can also be used to investigate short-range correlations, because sub-threshold K^+ probe the high momentum component of the nuclear wave function. It should be stressed that JLab and experimental Hall A is uniquely suited for the proposed experiment.

II. PHYSICS MOTIVATION: THE K^- MASS MODIFICATION IN THE NUCLEAR MEDIUM

The properties of strange mesons in a nuclear medium are essential to the understanding of strong interactions. According to various theoretical approaches, the K^+-nucleon potential in a medium is expected to be slightly repulsive while K^- mesons are expected to feel an attractive force in the nuclear medium [12] – [15]. These models also predict that the effective mass of the K^- decreases in a nuclear medium while the effective mass of the K^+ slightly increases and that there is a distinct difference in the nuclear density dependence of K^+ and K^- effective masses(Fig. 1). A decrease in the effective K^- mass would lead to an in-medium shift in the production threshold to a lower energy, implying an enhancement of the K^- yield over the K^+ yield at equivalent energies below the free-space threshold. The free-space photo-production thresholds for K^+ $(\gamma + p \rightarrow K^+ + \Lambda)$ and K^- $(\gamma + p \rightarrow K^+K^- + p)$ are 0.911 GeV and 1.506 GeV respectively, and the production of $K^\pm$ at equal energies above or below each respective threshold is referred to as *equivalent energy*. Fig. 2 shows the shift in the production threshold as a function of the ratio of the effective K^- mass to its free space mass.

The K^+ and K^- properties in the nuclear medium so far have been studied by

- nucleus nucleus (AA) collisions
- proton nucleus (pA) collisions

A. (AA) Collisions

Recently, a number of nucleus-nucleus collision experiments have observed about 1-2 orders of magnitude enhancement in the K^-/K^+ cross section ratio at beam energies below the free NN kaon production threshold (when plotted as a function of the equivalent energy) compared to nucleon-nucleon collision experiments near threshold. In addition the spectral slopes of the K^- mesons are steeper than those of K^+ at the same beam energy [11](Fig. 3).

This phenomenon has been observed in C+C, Ni+Ni, and Au+Au collisions. Fig. 3 shows the K^-/K^+ ratio as a function of C.M.-kinetic energy in C+C collisions, and one observes a steep decrease in the ratio with increasing kinetic energy. In contrast, transport calculations (cf. [16]) without in-medium mass modification, as a function of kinetic energy have failed to describe the data. A similar effect in the Ni+Ni system is shown in Fig. 4. Here the inclusive K^+ and K^- production cross-section is shown as a function of the c.m. kinetic energy. K^+ at 1.0 GeV/n and K^- at 1.8 GeV/n, are at equivalent energies below the NN production threshold. Note that $\sqrt{s} - \sqrt{s_{\rm th}} = -0.23$ GeV for both, because $\sqrt{s_{\rm th}} =$ 2.55 GeV for K^+ production ($p + p \rightarrow K^+ + \Lambda + p$) and 2.86 GeV for K^- production ($p + p \rightarrow K^-K^+ + p + p$). The cross-section of K^+ and K^- at these equivalent energies are almost equal ($K^-/K^+ \sim 1$). In striking contrast, for p+p system near threshold the K^-/K^+ ratio is < 0.1. Some of the theoretical models (see [17] and references therein) explain both these effects by incorporating the reduced effective mass of the K^- in the transport models, where the increased yield in K^- due to the reduced K^- effective mass overcompensates the absorption of K^- by strangeness exchange reactions. However, these measurements are indirect probes of the in-medium physics, since it is difficult to separate in-medium effects from other hadronic processes which affect the kaon production. Also it has been shown [18] that it is important to include higher resonances and kaon dynamics into the models. In heavy ion reactions secondary collisions often occur between resonant states, the excitation energy of these resonances is then available for particle production. Thus detailed effects of secondary collisions in nucleus-nucleus collisions need to be fully understood before the enhancement in production rates can be attributed to in-medium effects. Moreover, a recent article [19] on the in-medium modification of the K^- mass suggests that either the optical potential of the K^- becomes repulsive or the attraction is drastically reduced for finite K^- momenta or finite temperature, and hence the K^- mass does not decrease substantially in heavy ion collisions. The authors try to explain the observed enhancement of the K^- rates below threshold in terms of the enhanced production of K^- via pions and Σ hyperons. But there are still other models using the dispersion approach [20] which suggest that contrary to

Ref. [19], the K^- –N potential remains attractive even at high momenta. Thus it is important to employ an alternative experimental method to investigate the K^- production rates below the free NN production threshold and to investigate the finite momentum dependence of these production rates.

B. (pA) Collisions

One obvious approach in hadronic scattering to search for evidence of modification of K^- properties in the nuclear medium is proton nucleus scattering. Since most of the models (cf. Fig. 1) predict a significant change in the in-medium K^- mass even at normal nuclear density, these experiments present an independent study of the phenomenon of in-medium modifications of kaons. Moreover, pion hyperon reactions, which are believed to be the main source of K^- production in AA collisions, are suppressed [17] and therefore cannot account for possible enhanced yields. This has led to considerable activities in studying kaon production in p+A reactions. In general, the picture of a proton interacting with a light nuclear target is less complicated compared to nucleus-nucleus collisions. K^+ production in p+A collisions below the free-space production threshold has also been studied in recent years [21]- [24]. Most recently A. Badalà *et al* [25] have reported invariant cross-sections for sub-threshold K^+ production in p+C collisions and their results are in agreement with theoretical calculations which predict the dominance of multi-step processes at sub-threshold energies. Data on subthreshold K^- [26] production in p-A reactions have only been reported from ITEP, where such measurements were done a few years ago, and very recently from GSI [27]. The measurements from ITEP have reported [28] evidence for the modification of K^- mass in nuclear matter of normal density from their analysis of the sub-threshold K^- production. However, such an analysis depends on the total cross-section for K^- production in proton-nucleon collisions near threshold, which is not yet available with adequate precision. The preliminary results from GSI also show an enhanced K^-/K^+ ratio in p+Au collisions as compared to p+p collisions.

C. (eA) Collisions

Electroproduction of K^+ and K^- from nuclear targets provides an alternative probe of in-medium physics in which the effects of secondary production, which plague heavy ion experiments, are suppressed. Recent calculations of Sibirtsev *et al.* [38] have shown that the secondary production from pions is indeed negligible. It allows for the study of the finite momentum effect on the K^- production rates. Moreover, the $\gamma p \rightarrow K^+\Lambda$ cross-section has been shown to be two orders of magnitude larger [38] than the $pp \rightarrow K^+\Lambda p$ cross-section. This makes e+A scattering a more effective and cleaner probe of the in-medium mass modification of K^- particles than both A+A and p+A reactions.

The sub-threshold production rates are expected to be very sensitive to the in-medium masses [29] of the produced particles, and taking the ratio of the K^- and K^+ production rates removes many experimental uncertainties thereby reducing the systematic uncertainties and also makes theoretical calculations easier. However, the challenge of electroproduction is that the final state interactions (FSI), the interactions of $K^\pm$ with the rest of the nucleons in the nucleus before they exit the nuclear medium, need to be separated from the in-medium mass modification effect. One has to isolate the in-medium shift in the production threshold of the K^- from FSI We propose that such a separation can be achieved if one measures the $\frac{K^-}{K^+}$ ratio at equivalent energies below their respective free-production thresholds while detecting $K^\pm$ at the same momentum and then compare it with the $\frac{K^-}{K^+}$ ratio at equivalent energies above their free thresholds. Here the $K^\pm$ detected above threshold would also have the same momentum as those detected below threshold. Note that since the $K^\pm$ above and below the threshold all have the same momentum, the FSI effects of the K^+ below the free production threshold cancels with the FSI effects of the K^+ above the free production threshold. Similarly the FSI effects of the K^- above and below threshold cancel as well. Thus the super-ratio of $\frac{K^-}{K^+}$ at equivalent energies below the free production threshold to the $\frac{K^-}{K^+}$ at equivalent energies above the free production threshold, all measured at the same momentum can isolate the in-medium shifts in the production threshold from other nuclear

medium effects. We further elaborate on this scheme below.

The in-medium mass modifications can be addressed by comparing the sub-threshold production ratio to the above threshold production ratio of $\frac{\mathrm{K}^-}{\mathrm{K}^+}$ from a nuclear target (such as ^{12}C.) For equivalent sub-threshold energies (i.e. at similar $\sqrt{s} - \sqrt{s_{\rm th}}$ below the K^+ and K^- free space thresholds respectively) one can form the ratio

$$R_{\rm sub\_th}(^{12}\mathrm{C}) = \frac{\gamma^* + {}^{12}\mathrm{C} \rightarrow \mathrm{K}^- + \mathrm{X}}{\gamma^* + {}^{12}\mathrm{C} \rightarrow \mathrm{K}^+ + \mathrm{X}},$$

where the reactions on ^{12}C are below the respective thresholds and the K^+ and K^- have similar momenta. We will measure this ratio at equivalent energies below and above the threshold (e.g. 0.06 GeV below and 0.13 GeV above the K^+ threshold and 0.06 GeV below and 0.13 GeV above the K^- threshold) and compare them to the ratio of production rates from hydrogen. By factorizing out the FSI effect we can re-write the ratio above as

$$R_{\rm sub\_th}(^{12}\mathrm{C}) = R_0(^{12}\mathrm{C}) \times \frac{g^{\mathrm{K}^-}(\mathrm{p}_K)}{g^{\mathrm{K}^+}(\mathrm{p}_K)},$$

where $R_0(^{12}\mathrm{C})$ is the ratio of the rates including mass modification but no final state interactions, and $\mathrm{g}^{\mathrm{K}^\pm}(\mathrm{p}_K)$ is the effects due to FSI for K^- and K^+. Here we have used the approximation that FSI or re-scattering effects can be parametrized as a function of K^+ (K^-) momentum and atomic number of the target nucleus (i.e. $\mathrm{g} \equiv \mathrm{g}(\mathrm{p}_K, \mathrm{A})$ [30–32].)

If there is any reduction in the K^- mass it would push the K^- production threshold below its nominal value of 1.506 GeV thereby increasing the ratio $R_0(^{12}\mathrm{C})$ above its nominal value. Measuring the same ratio above threshold and detecting K^- and K^+ at the same momentum as below threshold gives,

$$R_{\rm above\_th}(^{12}\mathrm{C}) = R_0'(^{12}\mathrm{C}) * \frac{g^{\mathrm{K}^-}(\mathrm{p}_K)}{g^{\mathrm{K}^+}(\mathrm{p}_K)}.$$

Here the factors g for the K^- and K^+ respectively are the same as in the sub-threshold case because the $\mathrm{K}^\pm$ are of similar momentum above and below threshold (as mentioned above we have used the approximation that FSI is a function of K^+ (K^-) momentum and atomic number of the target nucleus only.) $R_0'(^{12}\mathrm{C})$ is the same quantity as $R_0(^{12}\mathrm{C})$ but

measured above threshold where it is quite insensitive to mass modification. This is because the production cross-section above threshold starts to become constant as a function of energy (cf. Fig. 15). From the last two equations we see that if there is any reduction in the K^- mass in the nuclear medium, we will have $\frac{R_0(^{12}C)}{R'_0(^{12}C)} > 1$ and one would observe an enhancement in the ratio $R_{sub\_th}(^{12}C)$ with respect to $R_{above\_th}(^{12}C)$. By detecting the K^+ and K^- above and below threshold at similar momentum we can ensure that the effect due to FSI are the same and hence any enhancement in $R(^{12}C)$ will be due to mass modification and not FSI. Being a super-ratio measurement there is no need to separate the $\gamma^* + {}^{12}C(p) \rightarrow K^+ + \Lambda + X$ from the $\gamma^* + {}^{12}C(p) \rightarrow K^+ + \Sigma + X$ events making the experiment insensitive to the resolution of the spectrometers.

In addition we can quantify the FSI effect in terms of the ratio of $R_{above\_th}(^{12}C)$ to $R(^1H)$, where $R(^1H)$ is the ratio of K^- to K^+ production from a proton target, which makes it free from the effects of mass modification as well as FSI. It is given by

$$R(^1H) = \frac{\gamma^* + p \rightarrow K^- + X}{\gamma^* + p \rightarrow K^+ + X} \;=\; R'_0(^1H). \qquad (1)$$

Since ^{12}C has both neutrons and protons this scheme relies on the isospin symmetry, whereby one expects that $\gamma^* p \rightarrow K^+K^-p$ and $\gamma^* n \rightarrow K^+K^-n$ have similar production rates. This assumption is supported by experimental data of Bebek *et al.* [33]

This also gives us an alternative scheme for quantifying the enhancement. One can use the ratio of K^+ and K^- production from ^{12}C and ^1H targets above threshold to determine the transparency for K^+ and K^- respectively. Using this transparency one can correct the sub-threshold ^{12}C data for FSI. And finally one can look for an enhancement in the corrected sub-threshold K^-/K^+ ratio from ^{12}C compared to the ratio from ^1H.

The sub-threshold K^- production rates will have very small contamination from the process $\gamma + p \rightarrow \phi^0 + p$ since the selected kinematics are well below the ϕ^0 production threshold. The above threshold rates will also have a small contamination from such processes because the ϕ^0 will still be produced below the free production threshold. Note that making the sub-threshold measurement at equivalent energies and similar momentum ensures that the

K^- and K^+ probe overlapping regions of the spectral function. Thus a measurement of the $\frac{K^-}{K^+}$ ratio at sub-threshold energies will be a big step towards verifying possible in-medium mass modifications.

D. Probing the Short-range Correlations

The sub-threshold K^+ production data collected during the experiment can also be used to extract the nuclear spectral function. The nuclear spectral function has been studied extensively in (e,e′p) reactions. However, the high momentum components of the spectral functions, which are believed to arise from short range two-nucleon correlations, have just begun to be accessible experimentally. Attempts have been made to probe these short range correlations with (e,e′p) and (e,e′pp) experiments. Sub-threshold production of K^+ from nuclei is a powerful alternative probe of these high momentum components and thus the short range correlations. Moreover, no additional beam time is needed for this study; the same data set which is used to study medium modification can be used to study short-range correlations.

The K^+ production threshold from $\gamma + p \rightarrow K^+\Lambda$ is 0.911 GeV. However, in nuclear medium the threshold is given by energy conservation as

$$(m_K + m_\Lambda)^2 = (E_\gamma + E_N)^2 - (\mathbf{k}_\gamma + \mathbf{q}_N)^2 \quad (2)$$

where $\mathbf{q}_N$ is the momentum of the nucleon inside the nucleus ($\mathbf{q}_N$=0 for free space) and E_N is the nucleon energy ($E_N = M_N$ for free space). Using this equation one can get the spectrum of nucleon momentum $\mathbf{q}_N$ and energy E_N available for $K^+\Lambda$ production, which depends on the photon energy E_γ. The free space dispersion relation is given by $E_N = \sqrt{q_N^2 + M_N^2}$. Figs. 5 and 6 show the range of nucleon momenta q_N and energies E_N (area within dashed lines) for which the reaction $\gamma p \rightarrow K^+\Lambda$ is allowed for photon energies of 0.7 GeV and 0.9 GeV respectively. The solid line is the dispersion relation in free space and the arrow shows the Fermi momentum for nuclear matter. This tells us that for E_γ about 0.2 GeV below the

free threshold of 0.911 GeV, the nucleon momentum $\mathbf{q}_{\rm N}$ must be greater than the Fermi momentum of ^{12}C (≈ 0.221 GeV) for the production of K^+. Thus K^+ electro-production is sensitive to the high momentum component of the nuclear wave function.

The short-range NN interactions induce correlations into the nuclear wave function; thus the nuclear momentum distribution has a tail for momentum greater than the Fermi momentum; $q_{\rm N} > q_F$ (Fig. 7). These tails as well as the nuclear dispersion relation can be investigated via electro K^+ production as described above. This is similar to the eA$\rightarrow$e$'$pX studies but has the added advantage of being sensitive only to the high momentum component of the spectral function. Although it also suffers from the problem of distortions due to final state interactions, these effects are relatively small because the K-N interaction is weak. This makes sub-threshold K^+ production a good probe of the high momentum components of the wave function and thus a good probe of the short range correlations. From the momentum distribution of the sub-threshold K^+, one can extract the strength of the carbon spectral function above the Fermi energy using the relation [38]

$$E_{\rm K}\left(\frac{d^3\sigma}{d^3p_{\rm K}}\right)_{\gamma^*{\rm C}\rightarrow{\rm KX}} = A_{\rm eff}(\sigma_{\rm KN})\int d^3q_{\rm N}\, dE_{\rm N}\, S(q_{\rm N},E_{\rm N})\frac{Z}{A}E'_{\rm K}\left(\frac{d^3\sigma_{\gamma^*{\rm p}\rightarrow{\rm KX}}(\sqrt{s})}{d^3p'_{\rm K}}\right), \qquad (3)$$

where $\sqrt{s}$ is the invariant energy of the incident virtual photon and the struck proton, and the limits of the integral are fixed by energy conservation as,

$$m_{\rm K}+m_\Lambda \leq \sqrt{s} \leq \sqrt{2\omega M_A + M_A^2} - M_{A-1}.$$

The factor $A_{\rm eff}$ is the effective primary collision number which quantifies the in-medium distortion of the K^+ while traveling through the nuclear target. Such an extraction would be a model dependent extraction of the spectral function.

E. Previous Data

At present some data exist for H(e,e$'K^+$) [34], [35], [36] and A(e,e$'K^+$) [36], [37] (all of which are from JLab) but no data exist for A(e,e$'K^-$), and all the existing data is above

threshold; this is primarily because of the short lifetimes ($c\tau_K$ = 370 cm), low production rates and high production thresholds, as well as inadequate particle identification capabilities for $K^{\pm}$. With the advent of very high luminosity CW machines such as JLab and the availability of better detector technologies, it has become possible to do these experiments with sufficient accuracy. Given the current lack of data on $K^{\pm}$ electroproduction from nuclear targets in the sub-threshold region, and the availability of a high duty factor high intensity electron beam at JLab and optimal detector packages already planned or in place in the spectrometers, it is highly desirable to do these measurements. Moreover, although technically very challenging, these sub-threshold measurements can be made only at JLab. In the following sections we will describe the proposed measurement, estimated counting rates and the required detector performances.

III. EXPERIMENT

A. Experimental Overview

We propose to perform A(e,e′K^+)X and A(e,e′K^-)X measurements on liquid hydrogen and solid carbon target. The schematic of the reaction is shown in Fig. 8. The experiment, being a coincidence experiment, relies on the 100% duty factor of the JLab electron beam. The scattered electron and $K^{\pm}$ will be detected in coincidence at forward angles using one of the HRS spectrometer in Hall A and a kaon spectrometer which will be discussed in detail in Section III.B . Electron beams with energies ranging from 1.6 - 4 GeV and energy transfers ranging from 0.8 to 1.2 GeV will be used. Since we want to avoid large momentum transfers where the kaon production rates are low, small scattering angles are necessary. It has been shown by Donnelly *et al.* [40] that the kaon rates decrease with the angle $\overline{\theta}_K$, where $\overline{\theta}_K$ is the kaon angle with respect to the incident beam direction. Thus both the electron scattering angle θ_e and the angle $\overline{\theta}_K$ will be kept small. The septum magnets will be used to access the desired forward angles. The coplanar geometry for the reaction is shown in Fig. 9.

The subthreshold production kinematics of the $K^{\pm}$ results in low momentum $K^{\pm}$. The kaon momentum ranges from 0.3 to 0.4 GeV. The threshold for K^+ electroproduction is $\omega = E_{\gamma^*} = 0.911$; thus energy transfers below 0.911 GeV are below the free production threshold of K^+. At these energies the measurement will be confined to the ^{12}C target only. The threshold for production of K^- in free space is $\omega = E_{\gamma^*} = 1.506$ GeV (from $\gamma p \rightarrow pK^+K^-$). Thus the K^- production will be measured at energy transfers (ω) < 1.506 GeV such that they are at equivalent energies below the threshold compared to the sub-threshold K^+ production. These measurements will also be performed with just the ^{12}C target. At these sub-threshold energy transfers the ratio of K^-K^+ as a function of kaon momentum will be formed. At energy transfers above 0.911 GeV for K^+ production and above 1.506 GeV for K^- production, the ratio of K^-/K^+ will be measured at equivalent energy transfers. Here too we will detect $K^{\pm}$ with momentum similar to those in the sub-threshold measurements. Above the free space production threshold we will make measurements on a solid ^{12}C as well as a LH_2 target. This will let us form the ratio of $H(e,e'K^-)/H(e,e'K^+)$ at equivalent energies above the production threshold and help to estimate the effect of FSI and also quantify any enhancement of the K^-/K^+ ratio in sub-threshold production from ^{12}C.

The K^+ can be identified and separated from the protons and π^+, and the K^- can be separated from the electron and π^- using the time of flight and aerogel detectors. The kaon spectrometer (discussed in Section III.B) will have a small flight path in order to minimize the effect of decay. In order to identify the $K^{\pm}$ this detector package will have an aerogel counter in addition to a TOF scintillator detector. For kinematics where the singles rates are very high the Čerenkov counter in the HRS and the aerogel counter in the kaon spectrometer can be put into the trigger to reduce the online trigger rate.

B. The Kaon Spectrometer

This experiment requires a detector package which must be placed close to the exit of the septum magnet on an appropriate support structure with adequate shielding around it.

This will ensure a short flight path for the $K^{\pm}$. The Enge split pole spectrograph is a large bend spectrometer with a short flight path; hence along with the septum magnet, it can act as the kaon spectrometer. Fig. 10 shows a CAD drawing [50] of the Enge magnet placed in Hall A at 15.5 degrees from the beamline. The septum magnet can be operated to bend the scattered beam by 9.5 degrees thus allowing $K^{\pm}$ scattered at 6 degrees with respect to the incident electron beam to be bent into the spectrometer. However, as seen in Fig. 10, there are some interferences with the beam line, the septum magnet, and the scattering chamber (shown by the arrows). While moving the Enge split pole magnet to Hall A is a feasible option, modifications to the beamline and the existing scattering chamber are necessary for this experiment. It should be pointed out that the BigBite spectrometer with its large acceptance is not a viable option because, a.) at the small angles it cannot be operated with the septum magnets. b.) If we move both spectrometers to larger angles, such as 13^0, where one would not have to use the septum and the gain in acceptance would be large enough to compensate for the drop in virtual photon flux, the large acceptance would entail a huge rate for the background protons ($>$ 5 MHz.) These high rates cannot be handled by the BigBite detectors.

The detectors needed for this spectrometer include a pair of wire chambers for tracking, a pair of hodoscope planes for a trigger and TOF, and an aerogel threshold Čerenkov detector. The $K^{\pm}$ need to be separated from $\pi^{\pm}$ and protons over a momentum range of 0.3-0.75 GeV/c. A TOF scintillator detector will be used to separate K^+ from the protons. The back plane of this detector will be placed about 2 m from the front plane. The 0.3-0.4 GeV/c protons will arrive about 15 ns after they reach the front plane as shown in Fig. 11. Thus by arranging the gate widths and the logic of the signals from the front and back plane so as to reject signals which are more than 15 ns apart one can reject a majority of the protons. Fig. 12 shows the arrangement of the trigger which will incorporate the TOF signal and thus enable a good real to accidental ratio and background rejection online. Alternatively, one can use the RF timing information along with TOF to the front plane of scintillators which will be $>$ 4 m away from the target. This method would not require

a second plane of scintillators and would provide about 30 ns separation between the K^+ and the protons. Furthermore, one can achieve a much better reals to accidentals ratio and background rejection offline, once the TOF from the target to the front panel and the energy deposited in the scintillators is used for p/K/π separation. Scintillators in TOF configuration have performed with better than 99.5% efficiency in several experiments carried out in Hall C and Hall A. This will help us achieve a $5-10\times10^2$ p/K separation online and a $1-5\times10^3$ p/K separation offline.

An aerogel Čerenkov detector with n = 1.10 will be used as an additional level of pion suppression. Aerogel has been shown to reach n $\approx$ 1.1 when it is baked [51]. Such a Čerenkov counter would fire for the π^+ but not K^+ during positive polarity running, and would fire for e^-, π^- but not K^- during negative polarity running. Aerogel Čerenkov detectors have been shown to perform background proton rejection with 98% efficiency in Hall C and Hall A. Such a detector will help improve the reals to accidentals ratio and make this experiment possible.

The Enge spectrograph has to be placed on the floor close to the septum magnet. The distance of the detector stack from the septum magnet is constrained by the required short flight path to the first plane of scintillators. Fig. 13 shows the survival fraction as a function of flight path for 0.3 and 0.4 GeV/c $K^\pm$. The estimated flight path for the configuration shown in Fig. 10 is about 4.8 m. Changes in this configuration are likely to increase the flight path.

Construction of a new detector system can be avoided if the detector stack planned for the Enge spectrograph [52] is used with a new aerogel Čerenkov detector and a second plane of scintillators. The planned Enge spectrograph detector stack will have a pair of wire chambers and one plane of scintillators with a timing resolution of 120 ps. This detector stack along with a new aerogel detector and a second wall of scintillators 2 m from the front plane, would be adequate for this experiment. The detectors can be placed on the floor on a support structure and shielded. A schematic of the experimental setup is shown in Fig. 14. The Enge split-pole magnet will be placed at 16.0 degrees with respect to the beam. The

septum magnet will be operated to provide a bend of 9.2 degrees (note that these numbers are slightly different from the numbers shown in Fig. 10 but they will make it slightly easier to fit the Enge in Hall A.) This will ensure that $K^{\pm}$scattered by 5.8–7.8 degrees will be detected in the Enge spectrograph.

C. ^{12}C(e,e′K) Rates and Kinematics

To calculate the coincidence rates we have utilized the near real photon electroproduction formula [40]

$$\frac{d^5\sigma}{d\Omega_{\rm e} d\Omega_{\rm K} dE_{\rm K}}{}^{\theta_{\rm e},\overline{\theta}_{\rm K} small}_{\rm (e,e'K)} = \frac{\alpha}{8\pi^2}\left[1+\left(\frac{\rm E'}{\rm E}\right)^2\right]\frac{1}{E_\gamma \sin^2(\theta_{\rm e}/2)}\left[\frac{d\sigma}{d\Omega_{\rm K}}\right]_{(\gamma,K)}, \qquad (4)$$

where $E_\gamma \sim q \sim \omega = E - E'$. The angles $\theta_{\rm e}$ and $\overline{\theta}_{\rm K}$ must be kept small; otherwise t becomes large and the cross-section decreases accordingly. The final electron energy E' should be large compared to the incident beam energy; this keeps the singles rates as low as possible and thus improves the reals to accidentals ratio. The $K^{\pm}$ should have enough momenta so that the decaying fraction is not too large.

We used the ^{12}C(γ,K) cross-sections calculated by Sibirtsev *et al* [43] with a ^{12}C spectral function to calculate the ^{12}C(e,e′K$^+$) coincidence rates. Fig. 15 shows the total cross-section as a function of E_γ while Fig. 16 shows the typical differential cross-section for $E_\gamma = 0.8$ GeV. The photo-production cross-section $\frac{d\sigma}{dp_{\rm K} d\Omega}$ at $\rm E_\gamma = 0.8$ GeV and $\rm E_\gamma = 0.9$ GeV were used to obtain $\frac{d\sigma}{dp_{\rm K} d\Omega}$ at $\rm E_\gamma = 0.811$ GeV and $\rm E_\gamma = 0.861$ GeV while the photo-production cross-sections at $\rm E_\gamma = 1.1$ GeV and $\rm E_\gamma = 1.2$ GeV were used to obtain the cross-section at $\rm E_\gamma = 1.151$ GeV. The $\frac{d\sigma}{dp_{\rm K} d\Omega}$ were then integrated over $\Delta \rm p_K$ around $\rm p_K = 0.3$ GeV/c and $\rm p_K = 0.4$ GeV/c respectively to obtain the $\frac{d\sigma}{d\Omega}(\gamma, K)$ at $\rm p_K = 0.3$ GeV/c and $\rm p_K = 0.4$ GeV/c. Finally the $\frac{d\sigma}{d\Omega}(\gamma, K)$ were used in Eq. 4 to obtain the (e,e′K$^+$) electro-production cross-section. The estimated cross-sections range from 2.0 – 8.0 nbarns/GeV/sr^2. The coincidence rates including kaon decay were obtained by,

$$R_{\rm coin} = N_{\rm e} N_{\rm targ} \frac{d^5\sigma}{d\Omega_{\rm e} d\Omega_{\rm K} dE_{\rm K}} \Delta\Omega_{\rm e} \Delta\Omega_{\rm K} \Delta E_{\rm K} \exp\Big(\frac{-M_K {\rm L}}{3.71 {\rm p_K}}\Big) Eff$$

where L is the flight path and Eff is the detector and spectrometer efficiency (assumed to be 0.9 .) Table I shows the estimated ^{12}C(e,e'K$^+$) rates assuming the Enge split pole spectrograph along with the septum magnet is used to detect the K$^{\pm}$. The path-length is expected to be about 4.8 m and the angular acceptance is 0.8 msrad ($\pm$ 20 mrad horizontal and $\pm$ 10 mrad vertical.) The beam current was taken to be 100 μA and a 500 mg/cm^2 carbon target was used. The Tables also show the equivalent energy $\sqrt{s} - \sqrt{s_{\rm th}}$.

Table III shows the ^{12}C(e,e'K$^-$) rates. The K$^-$ production rates were obtained by assuming that they would be 1/3 (a conservative estimate based on heavy ion results and calculations of electroproduction of ϕ^0 mesons at similar kinematics) of the K$^+$ rates at the equivalent energies above and below the production threshold.

D. The Singles Rates and Real to Accidental Ratios

The singles rates were estimated using an inclusive electron scattering code QFS [46] and a $\pi^{\pm}$, N electroproduction code EPC [47]. For the K$^+$ singles rates we used the integral of the (e,e'K) cross-section expressed as a function of W and Q^2, given by:

$$\frac{d\sigma}{d\Omega_{\rm K}} = \int dW^2 \int \Gamma' \frac{d\sigma^{\rm CM}}{d\Omega_{\rm K}} \frac{d(\cos\theta^{\rm CM})}{d(\cos\theta)} dQ^2,$$

where Γ' is the virtual photon flux. We used data from G. Niculescu *et al.* [48] and R. Mohring [49] to obtain $\frac{d\sigma^{\rm CM}}{d\Omega_{\rm K}}$ for Λ and Σ^0 production, and extrapolated them to our kinematics using the parameterization [33]

$$\frac{d\sigma^{\rm CM}}{d\Omega_{\rm K}}(Q^2, W) \propto \frac{p_{\rm K} e^{2.1t}}{W(W^2 - M^2)(Q^2 + a)^2},$$

where $a = 2.67$ for Λ production and $a = 0.79$ for Σ^0 production.

A numerical integration over W and Q^2 was performed, using the Gaussian integration method. The ranges of the integration were,

$$W_{min} = M_\Lambda + M_K \text{ (for } \Lambda \text{ production)}$$

or

$$W_{min} = M_{\Sigma} + M_K(\text{for } \Sigma \text{ production})$$

and

$$W_{max} = \sqrt{s} - M_e$$

and for each W in this range

$$Q^2_{min} = 2(E_e E_{e'} - p_e p_{e'})_{CM}$$

$$Q^2_{max} = 2(E_e E_{e'} + p_e p_{e'})_{CM}$$

The cross-sections were calculated for $\sigma(\gamma_v p \rightarrow \mathrm{K}^+\Lambda)$, $\sigma(\gamma_v p \rightarrow \mathrm{K}^+\Sigma^0)$ and $\sigma(\gamma_v n \rightarrow \mathrm{K}^+\Sigma^-)$, assuming that $\sigma(\gamma_v n \rightarrow \mathrm{K}^+\Sigma^-) = \sigma(\gamma_v p \rightarrow \mathrm{K}^+\Sigma^0)$ (from isospin symmetry and also supported by experimental data of Bebek *et al.* [33]), The calculated cross-sections $\sigma(e, \mathrm{K}^+)$ from a ^{12}C target ranged from 0.2 – 1.8 nbarns/srad. Using this we get the kaon singles rate, including kaon decay in Hz as,

$$R_{\mathrm{K}} = N N_{\mathrm{targ}} \frac{d\sigma}{d\Omega_{\mathrm{K}}} \Delta\Omega_K \exp\left(\frac{-M_K \mathrm{L}}{3.71 \mathrm{p_K}}\right) Eff$$

, where L is the flight path and Eff is the detector efficiency (taken as 0.9 .)

The estimated kaon singles rates from a ^{12}C target without taking into account any nuclear interaction are shown in Tables II and IV.

The coincidence and singles rates is used to calculate the real (R) to accidental (A) coincidence ratio using,

$$\frac{\mathrm{R}}{\mathrm{A}} = \frac{\mathrm{R_{coin}}}{\mathrm{R_e R_K} \tau_{\mathrm{resl}}}$$

where τ_{resl} is the coincidence time resolution (we use a typical value of 1 ns), $\mathrm{R_K}$ is the kaon singles rate, $\mathrm{R_e}$ is the electron singles rate and $\mathrm{R_{coin}}$ is the coincidence rate. The R/A ratios range from 0.6 – 7.3. This ratio can be further improved offline by using the RF pulse

timing information to determine the coincidence start time instead of the electron arm start time. Using this technique the coincidence time resolution would depend only on the timing resolution of the kaon spectrometer, thus providing a factor of 5 improvement in the R/A ratio.

E. Computer and Electronic Dead Times

The high electron and proton singles rates in this experiment suggests that certain kinematics may have high electronic dead time. At present the best estimate of the electronic dead time in Hall-A is 0.02/KHz [41] this would lead to 28% electronic dead time for the kinematics with the highest electron rates. However, currently Hall-A [41] plans to install a new system by early 2001 which would reduce the electronic deadtime by up to a factor of 4 - 5. This would bring down the dead time to more reasonable levels (< 6 - 7 %.)

The computer dead time in Hall-A is estimated to be 0.012%/Hz hence computer dead time should not pose any problem for this experiment.

TABLES

TABLE I. Kinematics and Rates for ^{12}C(e,e′K$^+$)

E	E'	$\sqrt{s}-\sqrt{s_{\rm th}}$	$\theta_{\rm e}$	$\overline{\theta}_{\rm K}$(set pt.)	$P_{\rm K}$	Coin Rate	$\frac{R}{A}$	$\frac{R}{A}$
(GeV)	(GeV)	(GeV)	(deg)	(deg)	(GeV/c)	(sec^{-1})	online	offline
1.710	0.890	-0.054	6	6.6(6.8)	0.3	0.0035	0.68	3.4
1.710	0.854	-0.032	6	5.9(6.8)	0.4	0.0065	0.48	2.4
2.5	1.349	0.134	6	6.9(6.8)	0.3	0.0055	2.8	14
2.5	1.349	0.134	6	6.9(6.8)	0.4	0.02	7.3	36

TABLE II. Singles Rates for ^{12}C(e,e′K$^+$)

E	E'	$\theta_{\rm e}$	$\overline{\theta}_{\rm K}$	$P_{\rm K}$	e$^-$	π^-	π^+	p	K$^+$
(GeV)	(GeV)	(deg)	(deg)	(GeV/c)	(sec^{-1})	(sec^{-1})	(sec^{-1})	(sec^{-1})	(sec^{-1})
1.710	0.890	6	6.6	0.3	1.4E+06	1.4E+04	0.7E+04	1.6E+05	3.7
1.710	0.854	6	5.9	0.4	1.3E+06	4.5E+03	4.0E+03	0.5E+05	10.4
2.5	1.349	6	6.9	0.3	0.7E+06	3.1E+03	7.7E+03	1.6E+05	2.8
2.5	1.349	6	6.9	0.4	0.7E+06	3.1E+03	4.6E+03	0.5E+05	3.9

TABLE III. Kinematics and Rates for ^{12}C(e,e′K$^-$)

E	E'	$\sqrt{s}-\sqrt{s_{\rm th}}$	$\theta_{\rm e}$	$\overline{\theta}_{\rm K}$(set pt.)	$P_{\rm K}$	Rate	$\frac{R}{A}$	$\frac{R}{A}$
(GeV)	(GeV)	(GeV)	(deg)	(deg)	(GeV/c)	(sec^{-1})	online	offline
3.245	1.842	-0.052	6	7.7 (6.8)	0.3	0.0012	3.0	15
3.245	1.800	-0.030	6	7.4(6.8)	0.4	0.0022	1.6	8
4.045	2.253	0.134	6	7.4(6.8)	0.3	0.0018	9	45
4.045	2.253	0.134	6	7.4 (6.8)	0.4	0.007	35	175

TABLE IV. Singles Rates for ^{12}C(e,e′K$^-$)

E	E'	θ_e	$\overline{\theta}_K$	P_K	e^-(e)	e^-(k)	$\pi^-(e)$	$\pi^-(k)$	K^-
(GeV)	(GeV)	(deg)	(deg)	(GeV/c)	(sec^{-1})	(sec^{-1})	(sec^{-1})	(sec^{-1})	(sec^{-1})
3.245	1.842	6	7.7	0.3	0.4E+06	2.3E+05	3.0E+03	8.0E+03	1.0
3.245	1.800	6	7.4	0.4	0.4E+06	1.8E+05	3.0E+03	4.0E+03	3.4
4.045	2.253	6	7.4	0.3	0.2E+06	1.8E+05	2.0E+03	1.0E+04	1.0
4.045	2.253	6	7.4	0.4	0.2E+06	1.4E+05	2.0E+03	4.0E+03	1.0

F. p(e,e′K) Rates and Kinematics

We have used the model of R. Williams, C-R. Ji and S. Cotanch [42] to calculate the rates for a 15 cm liquid hydrogen target and an average current of 70 μA, with solid angles of 3.7 msr and 0.8 msrad used for the electron and kaon spectrometers respectively. A flight path of 4.8 m is used for the $K^{\pm}$. The coincidence rates for the various kinematics are shown in Tables V and VII.

TABLE V. Kinematics and Rates for p(e,e′K$^+$)

E	E'	$\sqrt{s}-\sqrt{s_{th}}$	θ_e	$\overline{\theta}_K$ (set pt.)	P_K	Rate	$\frac{R}{A}$	$\frac{R}{A}$
(GeV)	(GeV)	(GeV)	(deg)	(deg)	(GeV/c)	(sec^{-1})	online	offline
2.5	1.349	0.134	6	6.9 (6.8)	0.75	0.06	50	-

TABLE VI. Singles Rates for p(e,e′K$^+$)

E	E'	θ_e	$\overline{\theta}_K$	P_K	e^-	π^-	π^+	p	K^+
(GeV)	(GeV)	(deg)	(deg)	(GeV/c)	(sec^{-1})	(sec^{-1})	(sec^{-1})	(sec^{-1})	(sec^{-1})
2.5	1.349	6	6.9	0.75	1.4E+05	1.0E+03	5.7E+03	4.5E+05	8.0

TABLE VII. Kinematics and Rates for p(e,e′K$^-$)

E	E'	$\sqrt{s} - \sqrt{s_{\rm th}}$	$\theta_{\rm e}$	$\overline{\theta}_{\rm K}$ (set pt.)	$P_{\rm K}$	Rate	$\frac{R}{A}$	$\frac{R}{A}$
(GeV)	(GeV)	(GeV)	(deg)	(deg)	(GeV/c)	(sec^{-1})	online	offline
4.045	2.253	0.134	6	7.4 (6.8)	0.56	0.027	300	-

TABLE VIII. Singles Rates for p(e,e′K$^-$)

E	E'	$\theta_{\rm e}$	$\overline{\theta}_{\rm K}$	$P_{\rm K}$	e$^-$(e)	e$^-$(k)	π^-(e)	π^-(k)	K$^-$
(GeV)	(GeV)	(deg)	(deg)	(GeV/c)	(sec^{-1})	(sec^{-1})	(sec^{-1})	(sec^{-1})	(sec^{-1})
4.045	2.253	6	7.4	0.56	3.7E+04	5.2E+04	2.5E+03	4.0E+03	2.6

IV. BEAM TIME ESTIMATES

The ratio of reals to accidentals was estimated by using the inclusive electron scattering code QFS [46] and $\pi^{\pm}$, N electroproduction code EPC [47] to calculate the singles rates. A coincidence timing resolution of 1 ns was used. At kinematics where the reals-to-accidentals ratio is very low, we will add PID (in the form of a Čerenkov and or Aerogel veto and a Time-of-Flight veto) to the trigger, which will reduce the product of the singles rates by a factor of 5.0×10^3 in case of the p/K^+ and π^-/K^- separation and 5.0×10^3 in case of e/K^- separation. These numbers improve further when the TOF to the front panel and the energy deposited in the scintillators is incorporated offline.

Using the estimated coincidence rates and a goal of 1000 coincident events for each kinematic setting, we have calculated the beam time requirements for each target as shown in Table IX. We request a total beam time of 774 hrs ($\sim$32 days) which includes 754 hours for the production run and 20 hours for the checkout run. One must note that due to FSI only a fraction of the 1000 coincident events will be detected. The K^+p, K^+n K^-p and K^-n cross-sections [44] were used to estimate the fraction of $K^{\pm}$ which can exit the target nuclei. The K^+ transparency was estimated to be 0.8 while the K^- transparency was estimated to be 0.4. This implies that the 1000 counts would be reduced to 800 K^+ and 400 K^- respectively. The statistical error of the measured super-ratio of $\frac{K^-}{K^+}$, below and above threshold will be $\approx$8.0%.

TABLE IX. Beam time Estimates

Target	Beam Energy	Equivalent energy	Beam Time
	GeV	GeV	hours
LH_2	2.5	+0.134	4.4
(K^+)			
LH_2	4.045	+0.134	13.6
(K^-)			
^{12}C	1.71	-0.055	80.0
(K^+)	1.71	-0.030	42
	2.5	+0.134	62.0
^{12}C	3.245	-0.055	240.0
(K^-)	3.245	-0.030	126
	4.045	+0.134	186.0
Calibrations			20.0
Total			774.0

V. PROJECTED RESULTS

The mass modification of K^- in the nuclear medium will push the production threshold down and enable K^- to be produced above threshold. Fig 17 shows the mass-modification needed for the each of the two sub-threshold points to be pushed above threshold. If the sub-threshold points are pushed above threshold, the ratio of $\frac{K^-}{K^+}$ is expected to be enhanced compared to the ratio $\frac{K^-}{K^+}$ without any mass modification. Since the kaon momenta are the same above and below threshold, the effect of FSI can be decoupled from the mass-modification. Statistical error of the super-ratio will be around 8% and the systematic errors will be negligible since we will be measuring a super-ratio where the systematic uncertainties will cancel.

The correlation tail of the nuclear spectral function can be probed by the subthreshold electroproduction of K^+ from nuclei. The region of the tail being probed in sub-threshold electroproduction from ^{12}C is shown in Figs. 18 and 19 . The region of the correlation tail covered by each of the two sub-threshold points is shown. It is clear that for the sub-threshold points the K^+ are produced only above the Fermi energy of carbon, which is the region where the spectral function is sensitive to short range correlations.

VI. COLLABORATION BACKGROUND AND RESPONSIBILITIES

This experiment will use the Hall A cryotarget, one of the HRS spectrometers, the septum magnets, the existing (currently in Hall C) Enge split pole magnet and a kaon detection system which can be fashioned from the planned Enge spectrograph detector stack. An aerogel threshold Čerenkov detector with n = 1.10 and a second plane of scintillators will have to be built. The group from MIT together with JLab and FIU have built a second aerogel detector for the hadron arm and have the necessary expertise in aerogel detectors. Members of this collaboration have performed many coincidence experiments in both Hall A and C, including coincidence electroproduction of K^+. Members of the collaboration

have extensive experience in running the cryotarget and building scintillator hodoscopes and aerogel Čerenkov detectors. Engineering support from JLab will be needed in the beam line and scattering chamber modifications and design of the two additional detectors and the support structure to place them on the floor of the hall. The JLab staff will provide the necessary experience with the beam line instrumentations and the spectrometers.

VII. ACKNOWLEDGEMENTS

We thank A. Sibirtsev for providing us with the calculations of the cross-sections for kaon photoproduction from ^{12}C. We thank John LeRose for doing the optics studies to determine the acceptance of the Enge magnet when placed in Hall A. We are also grateful to Alan Gavalya and John LeRose for studying the feasibility of placing the Enge magnet in the Hall A beamline. We thank L. P. Gan and L. Tang for providing us the transport deck for the Enge magnet and for many helpful discussions about moving the Enge magnet from Hall C to Hall A. We also thank W. Hinton for providing us the results of the Hall C feasibility study of K^+ electroproduction from nuclear targets.

FIGURES

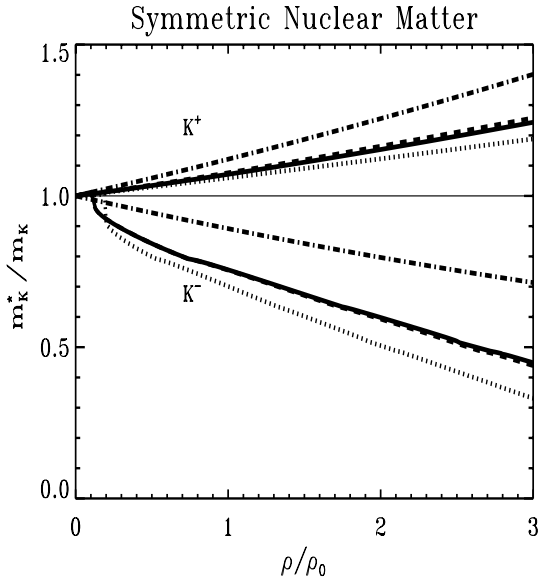

FIG. 1. Effective masses of K^+ and K^- in symmetric nuclear matter as a function of nuclear density $\rho = \rho_p + \rho_n$ in the unit of the nuclear matter density $\rho_o = 0.17 fm^{-3}$. The solid line is from ref [53] and include Pauli correlations. The dashed lines are results of in-medium coupled channel calculation from ref [54]. The dotted lines are calculations without Pauli correlations. The dashed-dotted line show the effective masses for the Tomozawa-Weinberg Born term only [53].

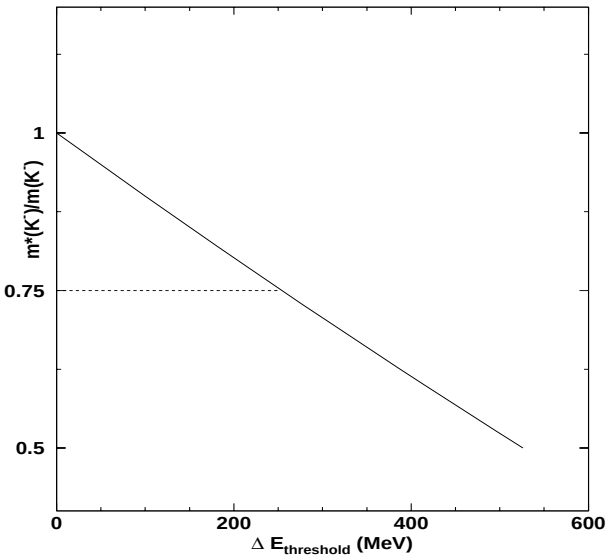

FIG. 2. The shifts in the K^- production threshold to lower energies with a decreasing K^- effective mass. Dashed line shows the predicted effective mass at normal nuclear density.

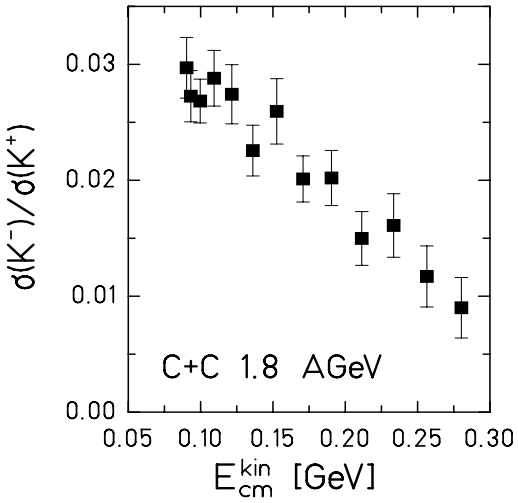

FIG. 3. K^-K^+ ratio as a function of the center-of-mass kinetic energy measured in C + C collisions at 1.8A GeV and at $\theta_{lab} = 40^o$.

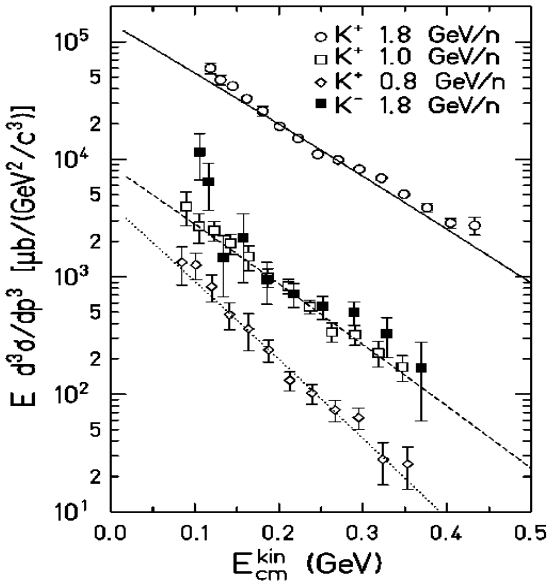

FIG. 4. K^- and K^+ inclusive cross-section as a function of the center-of-mass kinetic energy measured in Ni+Ni collisions. K^+ at 1.0 GeV/u (open squares) and K^- at 1.8 GeV/u (filled squares), are at equivalent energies below the NN production threshold ($\sqrt{s} - \sqrt{s_{th}}$ =-0.23 GeV for both.) Note that the cross-section for the K^- at 1.8 GeV/u is almost equal to that of K^+ at 1.0 GeV/u (these are at equivalent energies.)

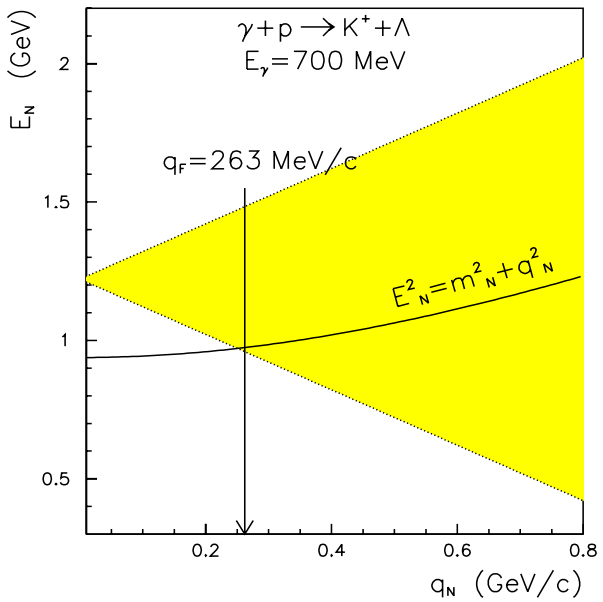

FIG. 5. The energetically allowed range (area between dashed lines) of nucleon momentum q_N and energies E_N for the $\gamma p \to K^+\Lambda$ reaction at photon energies of 700 MeV. The solid line indicates the dispersion relation in free space while the arrow shows the Fermi momentum for nuclear matter.

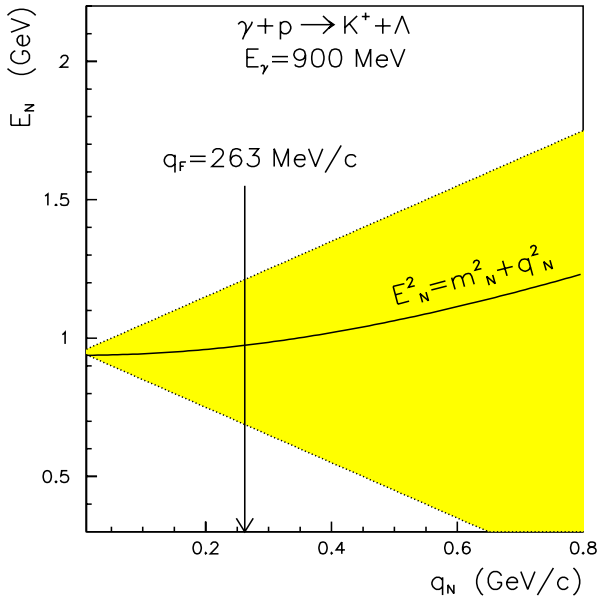

FIG. 6. The energetically allowed range (area between dashed lines) of nucleon momentum q_N and energies E_N for the $\gamma p \to K^+\Lambda$ reaction at photon energies of 900 MeV. The solid line indicates the dispersion relation in free space while the arrow shows the Fermi momentum for nuclear matter.

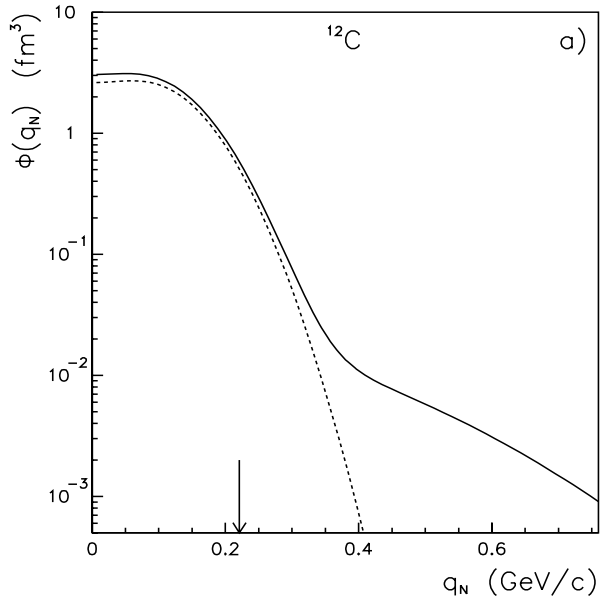

FIG. 7. The nucleon momentum distribution $\Phi(q)$ for ^{12}C taken from [39]. The dashed line shows the uncorrelated part, while the solid line is the sum of the uncorrelated and correlated parts. The arrow indicates the Fermi momentum for ^{12}C.

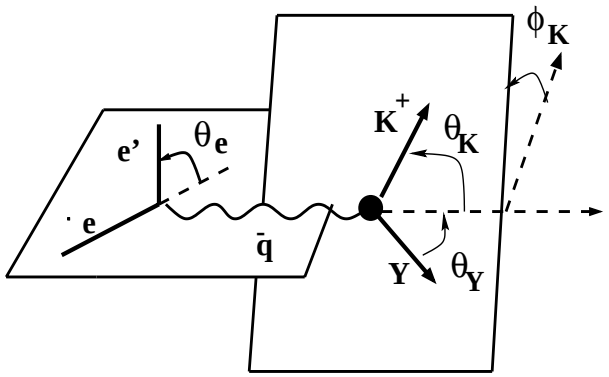

FIG. 8. Kinematics of the reaction.

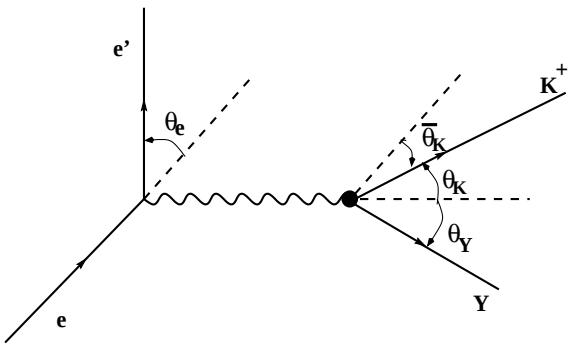

FIG. 9. Coplanar kinematics.

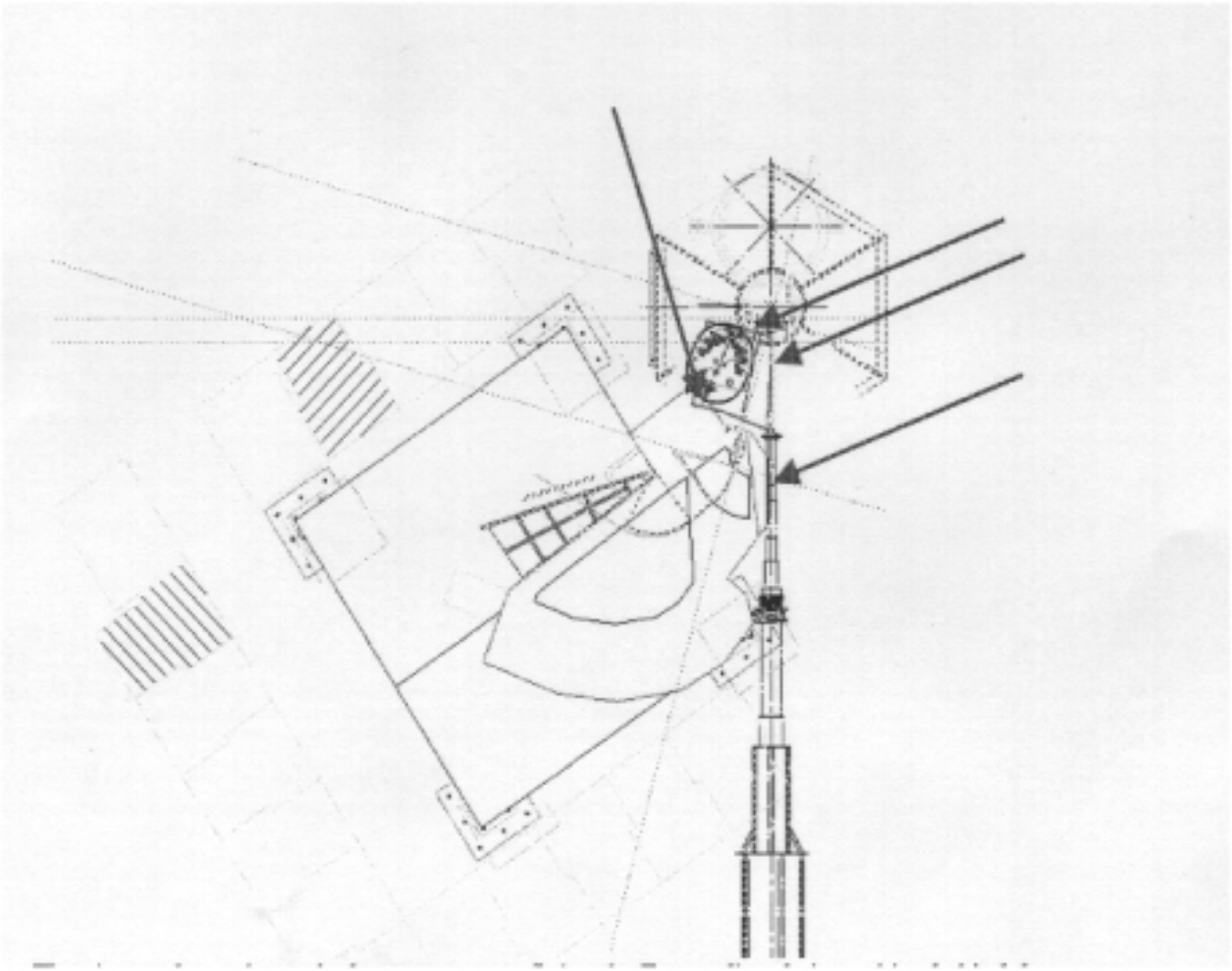

FIG. 10. Enge split pole magnet in Hall A. In this configuration trajectories centered around 6^0 scattering angle are bent by 9.5^0 by the septum and directed into the septum at 15.5^0. The arrows show the locations where the magnet yoke interferes with the beam-line, septum magnet and the scattering chamber. These interferences can be alleviated by changing the distance between the target and septum and between the septum and Enge, by modifying the scattering chamber and the septum magnet mount.

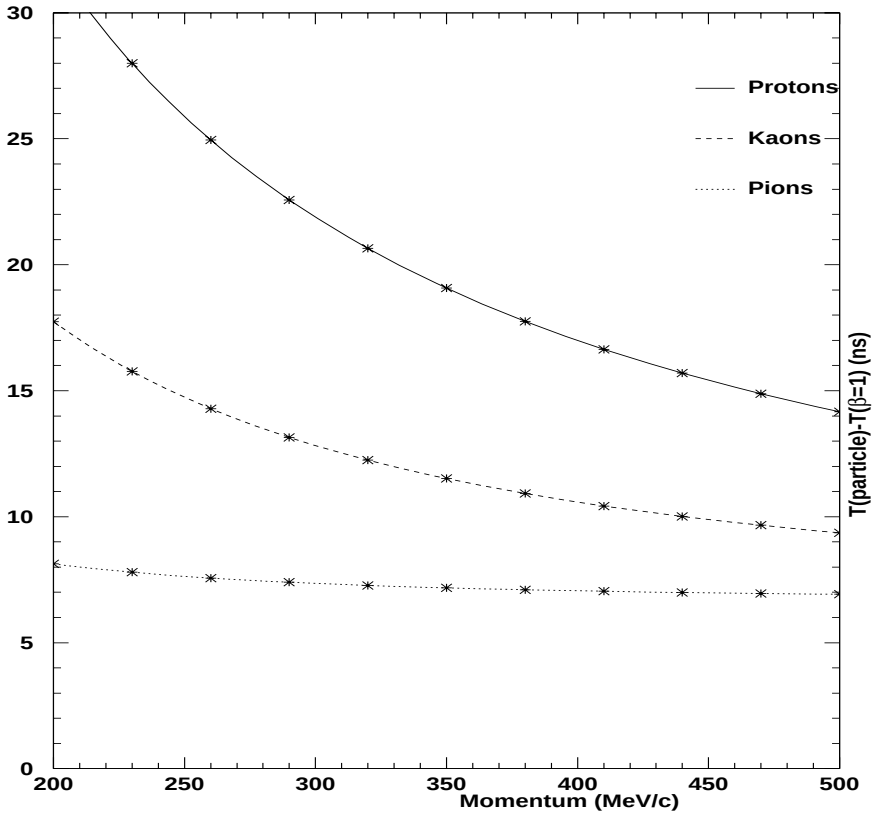

FIG. 11. The time of flight for protons, kaons and pions for a 2 m flight path.

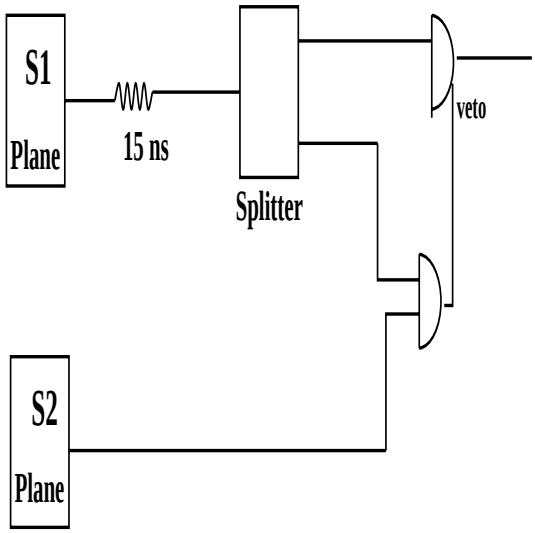

FIG. 12. The TOF trigger to reject protons. It rejects particles which hit both scintillator planes $>$ 15 ns apart.

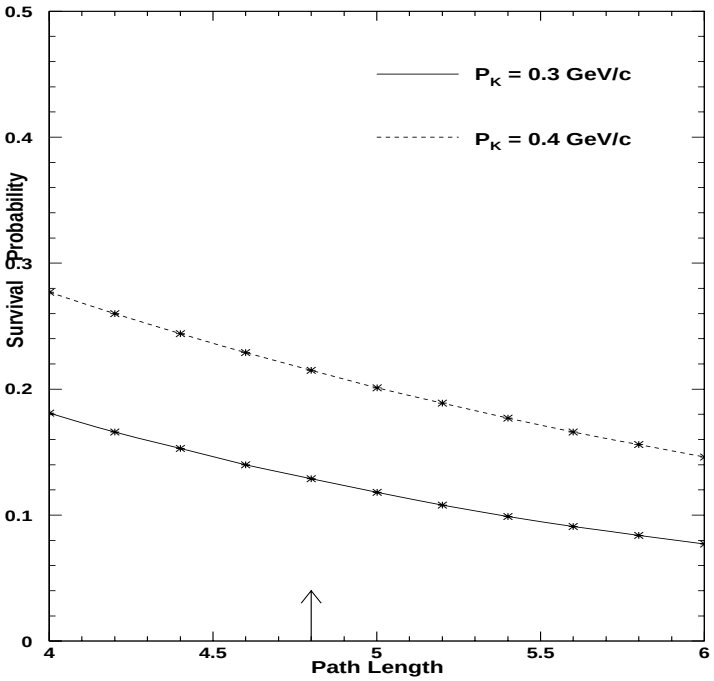

FIG. 13. Survival fraction of 0.3 and 0.4 GeV/c kaons as a function of flight path.

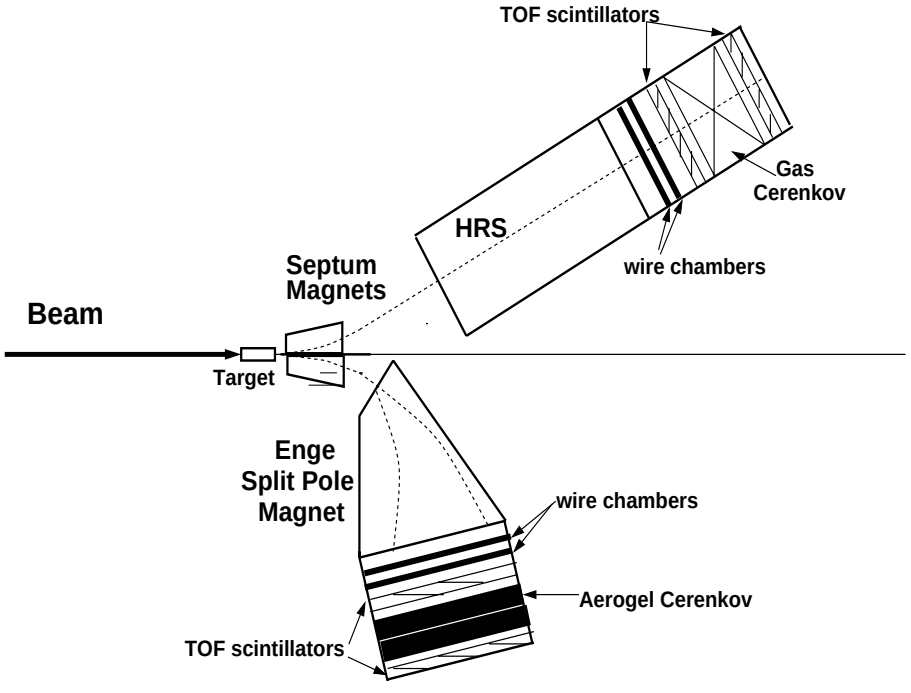

FIG. 14. A schematic of the experimental setup (not to scale).

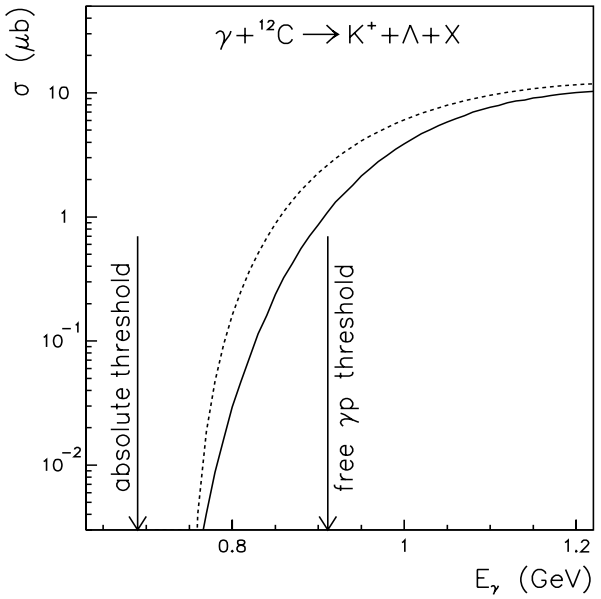

FIG. 15. The $\gamma C \to K^+ \Lambda X$ total cross-section as a function of photon energy E_γ. The absolute threshold arrow points to the minimum photon energy required to produce a K^+ from carbon, and the free γp threshold arrow points to the minimum photon energy needed to produce a K^+ from a proton in free space.

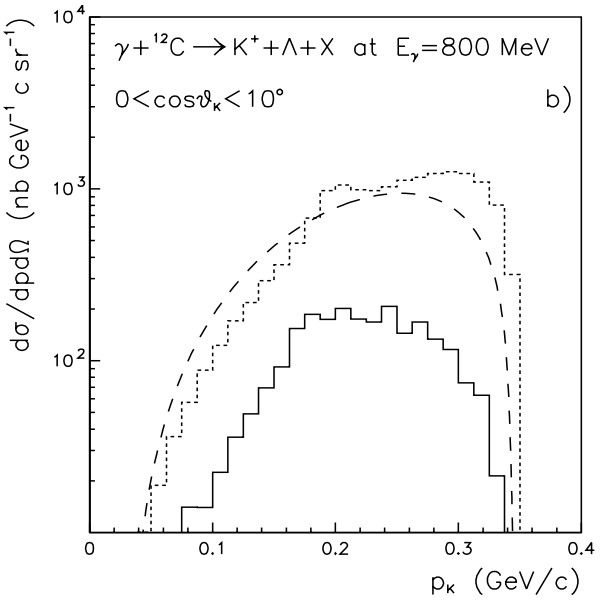

FIG. 16. The total momentum spectrum for the K^+ meson from the $\gamma C \to K^+ \Lambda X$ reaction at photon energy E_γ of 800 MeV. The solid line corresponds to calculation using the spectral function while the long dashed line is for calculation with the spectral function multiplied by a factor of 6 and the dotted line is for the Fermi gas model.

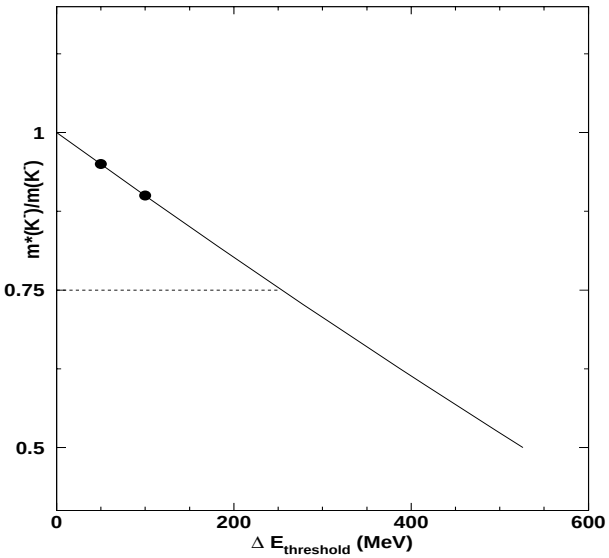

FIG. 17. The mass modification needed for the sub-threshold points to be pushed above threshold.

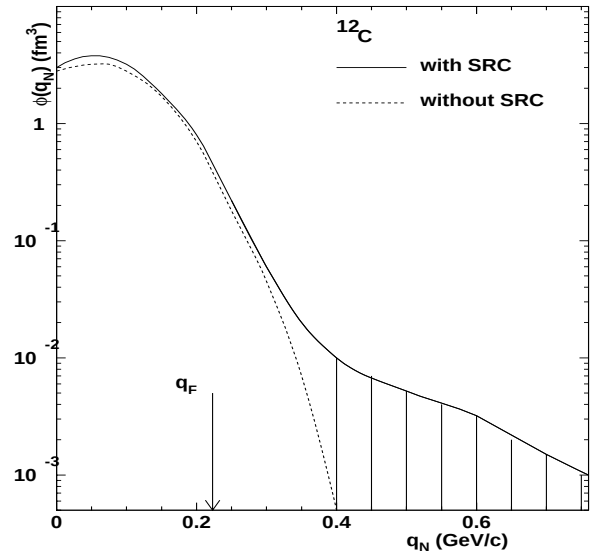

FIG. 18. The region of the ^{12}C spectral function probed in ^{12}C(e,e$'$K$^+$) for $E_{\gamma^*} = 0.811$ GeV and $P_K = 0.3$ GeV/c.

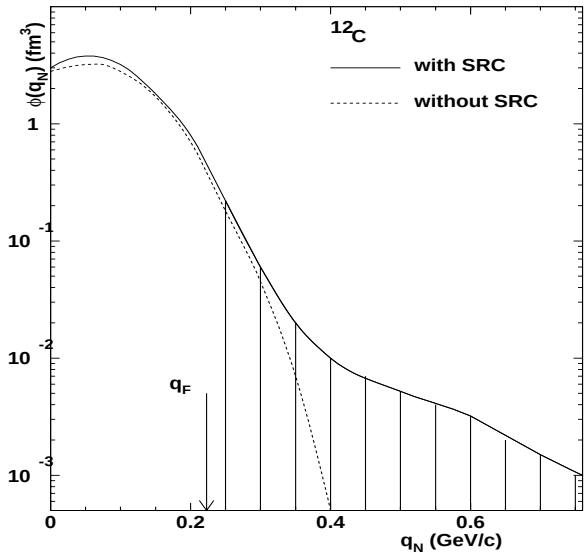

FIG. 19. The region of the ^{12}C spectral function probed in ^{12}C(e,e$'$K$^+$) for E$_{\gamma^*}$ = 0.861 GeV and P$_K$ = 0.4 GeV/c.

REFERENCES

[1] D. B. Kaplan and A. E. Nelson, Phys. Lett. B **175**, 57 (1986).

[2] G. E. Brown *et al.*, Phys. Rev. D**37**, 2042 (1988).

[3] G. E. Brown *et al.*, Phys. Lett. B**192**, 272 (1987).

[4] J. Schaffner *et al.*, Phys. Lett. B**334**, 268 (1994).

[5] M. Lutz *et al.*, Nucl. Phys. A**574**, 755, (1994)

[6] G. E. Brown *et al.*, Nucl. Phys. A**567**, 937 (1994).

[7] G. E. Brown and H. A. Bethe, Astrophys.Journ. **423** 659 (1997)

[8] G. E. Brown *et al.*, Phys. Rev. Lett.**60**, 2723 (1988).

[9] E. Friedman *et al.*, Nucl. Phys. A**625**, 272 (1997).

[10] E. Friedman *et al.*, Nucl. Phys. A**579**, 518 (1994).

[11] F. Laue *et al.*, Phys. Rev. Lett.**82**, 1640 (1999).

[12] R. Stock, Phys. Rep. **135**, 259 (1986).

[13] G. E. Brown *et al.*, Phys. Rev. C**43**, 1881 (1991).

[14] S. Klimt *et al.*, Phys. Lett. B**249**, 386 (1990).

[15] J. Aichelin and C. M. Ko, Phys. Rev. Lett.**55**, 2661 (1985).

[16] G. Q. Li, C. M. Ko and G .E. Brown, Phys. Lett. B**381** 71 1996

[17] W. Cassing and E.Bratkovskaya Phys. Rep. **308**, 65 (1999).

[18] M. Lutz, Phys Lett **B 426**, 12 (1998).

[19] Schaffner-Bielich *et al.*, Nucl. Phys. A**669**, 153 (2000).

[20] A. Sibirtsev and W. Cassing, Nucl. Phys. A**641**, 476 (1998).

[21] A. Shor *el al.*, Nucl. Phys. A**514**, 717 (1990).

[22] W. Cassing *et al.* Phys. Lett. B**359**, 29 (1990).

[23] A. Sibirtsev, Phys. Lett. B**359**, 29 (1995).

[24] A. V. Akindinov it et al., Heavy Ion Physics **4**, 325 (1996).

[25] A. Badalà *et al.*, Phys. Rev. Lett.**80**, 4863 (1998)

[26] A. V. Akindinov it et al., ITEP preprint 41-99, (1999).

[27] W. Scheinast for the KAOS collaboration, Act. Phys. Pol B Vol 31, 2305 (2000).

[28] Y. Kiselev *et al.*, J. Phys. G **25**, 381 (1999).

[29] X. S. Fang it et al., Nucl. Phys. A**575**, 766 (1994).

[30] V. F. Peresdov and L. S. Zolin, Physica Scripta **48**, 210 (1993).

[31] W. Zwermann *et al.*, Phys. Lett. B**145**, 315 (1984).

[32] J. Knoll and J. Randrup, Nucl. Phys. A**324**, 445 (1979).

[33] C.J.Bebek *et al.*, Phys. Rev. D**15**, 3082 (1977).

[34] G. Niculescu *et al.*, Phys. Rev. Lett.**81**, 1805 (1998).

[35] B. Zeidman, Jlab experiment E91-016, proposal, (1991)

[36] W. Hinton, private communication.

[37] L. G. Tang, Jlab experiment E89009, proposal, (1989)

[38] A. Sibirtsev *et al.*, LANL preprint server, nucl-th/990928

[39] C. Ciofi degli Atti and S. Simula, Phys. Rev. C**53**, 1689 (1996).

[40] T. W. Donnelly and S. R. Cotanch, Research Program at CEBAF Report of the 1985 Summer Study Group, CEBAF, 1985.

[41] R. Michaels private communication.

[42] R. Williams, C.-R. Ji and S. Cotanch, Phys. Rev. C**46**, 1617 (1992).

[43] A. Sibirtsev, private communication

[44] *Review of Particle Properties* Phys. Rev. D**45** (1992).

[45] W.L. Hinton, private communication

[46] J. W. Lightbody Jr. and J. S. O'Connell, NBS

[47] J. S. O'Connell and J. W. Lightbody Jr., NBS

[48] G. Niculescu, Ph.D. Thesis, Hampton University, 1998 (Unpublished).

[49] R. Mohring, Ph.D. Thesis, University of Maryland, 1999 (Unpublished).

[50] J. LeRose, private communication.

[51] R. K. Bock and A. Vasilescu, *The Particle Detector Briefbook*, Springer Physics (1998).

[52] L. Tang, private communication.

[53] T. Waas *et al.*, Nucl. Phys. A**617**, 449 (1997).

[54] T. Waas *et al.*, Phys. Lett. B**379**, 31 (1996).